https://doi.org/10.5194/acp-2021-892
Preprint. Discussion started: 17 November 2021

Atmospheric Chemistry and Physics Discussions

In-situ observation of warm atmospheric layer and the contribution of suspended dusts over the Tarim Basin

Chenglong Zhou[1,2,3], Yuzhi Liu[1, 2*], Qingzhe Zhu[1], Qing He [3], Tianliang Zhao[4], Fan Yang[1,2,3], Wen Huo[3], Xinghua Yang[3], Mamtimn Ali[3]

[1]Key Laboratory for Semi-Arid Climate Change of the Ministry of Education, College of Atmospheric Sciences, Lanzhou University, Lanzhou, 730000, China
[2]Collaborative Innovation Center for Western Ecological Safety, Lanzhou University, Lanzhou, 730000, China
[3]Institute of Desert Meteorology, China Meteorological Administration/Taklimakan National Station of Observation and Research for Desert Meteorology in Xinjiang/Taklimakan Desert Meteorology Field Experiment Station, China Meteorological Administration, Urumqi 830002, China
[4]Collaborative Innovation Center on Forecast and Evaluation of Meteorological Disasters, Key Laboratory for Aerosol-Cloud-Precipitation of China Meteorological Administration, Nanjing University of Information Science and Technology, Nanjing 210044, China
Correspondence to: Yuzhi Liu (liuyzh@lzu.edu.cn)

https://doi.org/10.5194/acp-2021-892
Preprint. Discussion started: 17 November 2021

Atmospheric Chemistry and Physics Discussions

Abstract. Basing on the radiosonde observations in the spring and summer during 2016-2017, an anomalous warm atmospheric layer is verified and the contribution of suspended dusts over the Tarim Basin (TB) is quantified. The result indicates a warm atmospheric layer between 300 hPa and 500 hPa with an average intensity of 2.53 K and 1.39 K in the spring and summer, respectively. Over the TB, where the world's second largest moving desert, the Taklimakan Desert (TD) is distributed, large amounts of dust particles are emitted from the TD and suspended over the TB. Using the Cloud-Aerosol Lidar and Infrared Pathfinder Satellite Observations (CALIPSO) data, we found the dusts can be lifted to the upper atmospheric layer between 2.5 and 5.5 km above mean sea level over the TB. Consequently, the suspended dusts can exert a maximum heating effect of approximately +0.45 K and +0.25 K in spring and summer, respectively. The contribution of dust heating to the anomalous warm atmospheric layer over the TB is 13.77% and 10.25% in spring and summer, respectively. In view of the topographical feature, the TB is adjacent to the Tibetan Plateau (TP) which acts as an elevated heat source in spring and summer. The warm atmospheric layer over the TB seems a northward extension of Tibet heat source, the concept of which is proposed in this study. Such a northward extension of the elevated heating by the Tibetan Plateau could induce some profound impacts on the regional climate, especially on the western section of the "Silk Road Economic Belt", and therefore demands more attention.

Keywords: Suspended dust, Heat source, Northward extension, Tibetan Plateau, Tarim Basin

https://doi.org/10.5194/acp-2021-892
Preprint. Discussion started: 17 November 2021

Atmospheric Chemistry and Physics Discussions

1 Introduction

The Tarim Basin (TB), which neighbors the Tibetan Plateau (TP) located to the south, covers an area of 5.3×10^5 km^2 and contains the Taklimakan Desert (TD), which occupies the main part of the TB and is one of the major dust sources in Asia (Gong et al., 2003; Wang et al., 2005). Basing on Cloud-Aerosol Lidar and Infrared Pathfinder Satellite Observations (CALIPSO) data, Liu et al. (2019) pointed out that large amounts of dust particles were emitted from the TD. Moreover, it was found that dust over the TB can be suspended for long time (Huang et al., 2008; Ge et al., 2014; Cheng et al., 2020). Therefore, it is an important issue to investigate the distribution of suspending dusts and impacts on the Earth-climate system.

Dust is one kind of the absorption aerosols, which absorbs radiation and heats the atmosphere (Yang et al., 2009). It can change the vertical distribution of radiation energy, and then affect the global and regional climate (Huang et al., 2011). The atmospheric layer is heated where the dust is suspended (Huang et al., 2006a, 2006b; Huang et al., 2015; Liu et al., 2014; Jia et al., 2018). The radiative forcing of dust over the TB and its feedback on climate change in Central Asia are a series of scientific issues that need to be further clarified. Hence, quantifying the heating induced by dust in the upper atmosphere over the TB is necessary.

About the radiative effect of suspending dusts over the TB, previous studies mainly based on the satellite observation and numerical model. Using CALIPSO data, Huang et al. (2009) found the significant radiative forcing and heating effect due to dusts over the part of the TB. Gu et al. (2006, 2016) and Law et al. (2006) present some numerical results to elucidate the dust's impact on air temperature at upper layers. However, focusing on above topic, the evidence from in-situ observations is lack.

https://doi.org/10.5194/acp-2021-892
Preprint. Discussion started: 17 November 2021


Atmospheric Chemistry and Physics Discussions

In this study, ground-based radiosonde observations, reanalysis and satellite data in spring and summer during 2016-2017 are employed to investigate the vertical distribution of the air temperature and the three-dimensional structure of suspended dust over the TB. Furthermore, the heating effect of suspended dust on the atmosphere is quantified. At last, the concept of the northward extension of Tibetan heat source is proposed.

The rest of the paper is organized as follows: section 2 describes the data and methodology used in the study. Section 3 presents the main results and discussion. Conclusions are given in section 4.

2 Data and Methodology

2.1 Radiosonde data

In this study, radiosonde data obtained from 6 radiosonde stations in the Tarim Basin (TB) (Fig. 1), including Kashi (KS), Akesu (AKS), Kuerle (KEL), Ruoqiang (RQ), Minfeng (MF) and Hetian (HT), acquired in spring and summer during 2016-2017 are used to obtain temperature profiles. During the radiosonde observations, temperature profiles were measured twice a day (08:00 and 20:00 UTC+8). The temporal resolution of the radiosonde data is 1 minute. Then we process the radiosonde data into monthly averaged at intervals of 25 hPa from 850 hPa to 200 hPa through the calculation. Simultaneously, weather phenomenon records from the ground-based meteorological stations are used for classification and statistics of the dusty weather all 6 stations (KS, AKS, KEL, RQ, MF and HT).

2.2 Reanalysis data

The Fifth-Generation European Centre for Medium-Range Weather Forecasts (ECMWF) Reanalysis (ERA-5) and Modern-Era Retrospective Analysis for Research and Applications, Version 2 (MERRA-2) reanalysis data in spring and summer during 2016-

https://doi.org/10.5194/acp-2021-892
Preprint. Discussion started: 17 November 2021


Atmospheric Chemistry and Physics Discussions

2017 are used. The ERA-5 reanalysis data in this study have a 0.5°×0.5° latitude/longitude spatial resolution and 37 pressure levels in the vertical direction. The MERRA-2 data are collected on a regular latitude-by-longitude grid of 0.5°×0.625° with 42 pressure levels in the vertical direction. The temporal resolutions of the temperature from the two sets of reanalyzes are 1 month. The ERA-5 data are the latest global atmospheric reanalysis produced by the ECMWF based on the Integrated Forecasting System (IFS) Cy41r2 (Hersbach et al., 2020). Notably, the ERA-5 data are generated from an ECMWF IFS spectral model and do not yet assimilate the impact of aerosols on meteorology (Simmons, 2006). The MERRA-2 data are the update of NASA's previous satellite reanalysis system and include additional observations and improvements to the Goddard Earth Observing System, Version 5 (GEOS-5) Earth system model (Randles et al., 2017). Unlike the ERA-5 data, the MERRA-2 data include the impact of dusts on meteorology (Gelaro et al., 2017).

2.3 Satellite data

Cloud-Aerosol Lidar and Infrared Pathfinder Satellite Observations (CALIPSO) was launched on April 28, 2006 to study the impact of clouds and aerosols on the Earth's radiation budget and climate. The CALIPSO satellite comprises three instruments, the Cloud-Aerosol Lidar with Orthogonal Polarization (CALIOP), the Imaging Infrared Radiometer (IIR), and the Wide Field Camera (WFC). In this study, the CALIPSO Level 1B and Level 2 Vertical Feature Mask (VFM) data sets (aerosol profile), which contain a half-orbit (day or night) of calibrated and geolocated single shot (highest resolution) Lidar profiles, were used to detect dust events. The CALIPSO Level 1B product provides the profiles of the total attenuated backscatter at 532 and 1064 nm; the feature classification from CALIPSO Level 2 VFM was used to distinguish the types of aerosols. Meanwhile,

https://doi.org/10.5194/acp-2021-892
Preprint. Discussion started: 17 November 2021


Atmospheric Chemistry and Physics Discussions

the seasonally averaged CALIPSO Level 2 VFM product was used to identify the dust profile top height.

2.4 Method of distinguishing the anomalous warm atmospheric layer

First, based on the radiosonde temperature data from each observation station in the TB in spring and summer during 2016-2017, the temperature can be fitted by the following equation:

$$T_F = aH + b \quad (1)$$

Where, T_F is the fitting temperature (℃), a is the mean slope, H is the altitude (hPa), and b is a constant. Then, according to Eq. (1), the fitting temperature profile can be calculated from the altitude data. Table 1 shows the fitting equations of each station.

The temperature difference (ΔT) is calculated by comparing the radiosonde measurements with the temperature computed from the fitting equation.

$$\Delta T = T_O - T_F \quad (2)$$

Where, T_O is the radiosonde temperature, T_F is the fitting temperature based on the Eq 1. This method serves as a good indicator of the anomalous temperature variation. A positive value means that the atmosphere is heating, while a negative value means that the atmosphere is cooling. The absolute value represents the intensity.

2.5. Method of estimating the dust effect on the temperature

In the analysis, the dust effect on the temperature is estimated based on the observation minus reanalysis (OMR) method proposed by Ding et al. (2013, 2016).

$$OMR = T_O - T_R \quad (3)$$

Where, T_O is also the radiosonde temperature, T_R is the ERA-5 temperature, which does not include the impact of dust aerosols and assimilates only limited upper atmospheric measurement data (Simmons, 2006). Therefore, this method serves as a good

https://doi.org/10.5194/acp-2021-892
Preprint. Discussion started: 17 November 2021


Atmospheric Chemistry and Physics Discussions

indicator of the dust heating. A positive value means that the atmosphere is heating, while a negative value means that the atmosphere is cooling. The absolute value represents the intensity.

3 Results and discussions

3.1 Anomalous warm layer over the TB

In the troposphere, the atmospheric temperature (hereinafter referred to simply as temperature) generally decreases linearly with increasing altitude. However, the temperature shows an anomalous temperature lapse rate over the TB. Figs. 2a-2f present profiles of the temperature difference (ΔT) between the radiosonde observations and the mean temperature rate calculations (see Section 2) at the observation stations, namely, Kashi (KS), Akesu (AKS), Kuerle (KEL), Hetian (HT), Minfeng (MF), and Ruoqiang (RQ), located in the TB in spring and summer during 2016-2017. Positive and negative values indicate warming and cooling, respectively. A relatively warm layer is observed between 700 hPa and 300 hPa in the spring and summer over the TB (shading in Figs. 2a-2f). However, the temperature difference presents obvious discrepancies among the stations. According to the location of 6 observational stations, as shown in Fig. 1, we divide the TB into north (KS, AKS and KEL) and south (HT, MF and RQ) region. In the north of the TB, although the height of the warm layer is consistent in both seasons, the warming is more intense in spring than in summer. Comparatively, in the south of the TB, the warming phenomenon extends to higher altitudes in summer than in spring, with greater warming at an altitude of more than 400 hPa.

In this study, we focus mainly on the temperature anomalies at altitudes of 500-300 hPa. The mean values of ΔT between 500 hPa and 300 hPa at each station in spring and summer are shown in Figs. 3a and b, respectively. In spring, the values of ΔT at each

https://doi.org/10.5194/acp-2021-892
Preprint. Discussion started: 17 November 2021


Atmospheric Chemistry and Physics Discussions

station are positive and range from 2.29 K to 2.73 K, with a mean value of 2.53 K. In comparison, ΔT is smaller in summer than in spring, varying from 1.21 K to 1.57 K, with a mean value of 1.39 K. Overall, an anomalous warm layer is measured at altitudes between 500 hPa and 300 hPa over the TB.

3.2 Distribution of dust aerosols in the warm layer over the TB

Dust aerosols are the principal particulate type in the atmosphere over the TB (Cheng et al., 2020). The distribution of dust aerosol is the key factor to evaluate its radiation forcing. In the following, the vertical distribution and variation of dust are analyzed based on the Level 1B and Level 2 Vertical Feature Mask (VFM) data sets over the TB from Cloud-Aerosol Lidar with Orthogonal Polarization (CALIOP). The distribution of the dust profile top height over the TB is also presented.

The product of CALIPSO, which can observe aerosols over bright surfaces and beneath thin clouds in clear skies (Vaughan et al., 2004; Winker et al., 2006), was used to identify dust aerosols. With a total attenuated backscatter coefficient at 532 nm and classified particles from CALIPSO were combined to identify dust aerosols. To identify dust aerosols, values of 0.0008-0.048 km^{-1} sr^{-1} was chosen as the thresholds of the total attenuated backscatter (Liu et al., 2015; Jia et al., 2015). Fig. 4 (left panels) shows the CALIPSO orbit-altitude cross-section of the 532-nm total attenuated backscattering coefficient on 4 July, 5 July, 25 July and 27 July 2016 along the CALIPSO trajectory presented in Fig. 1. The gray shading in Fig. 4 indicates the topography, and the deep blue area denotes the absence of signal due to clouds, which the laser cannot penetrate. As shown in Fig. 4 (left panels), the total attenuated backscatter ranged from 0.002 to 0.005 km^{-1} sr^{-1}. Based on the thresholds for identifying dust aerosols, 4 July and 5 July 2016 are considered two severe dusty days. Meanwhile, the dust layer can also be distinctly

https://doi.org/10.5194/acp-2021-892
Preprint. Discussion started: 17 November 2021


Atmospheric Chemistry and Physics Discussions

identified during the clear day, however, the range and intensity is relatively smaller compared with the dusty day.

CALIPSO data reveals that vertically extended dust layers are widespread throughout the TB with peak lidar returns between 2.5 and 5.5 km above mean sea level (MSL) due to the strong convective activity during the dusty and clear day (Cheng et al., 2020). The results were consistent with other studies (Huang et al., 2009; Liu et al., 2015). Fig. 4 (right panels) also describes the thick dust plumes are observed over the entire TB. Moreover, the geographic setting of the basin, surrounded by high mountains, generates atmospheric circulations in the basin that are favorable for dust to remain suspended in the air for a long time (Tsunematsu et al., 2005).

Fig. 5a plots the frequencies of dust events observed by ground stations in spring and summer during 2016-2017 throughout the TB. In spring, the frequencies of dust events are 55.43%, 50.00%, 53.26%, 33.70%, 22.83% and 34.24% in MF, HT, RQ, KS, KEL and AKS respectively. In summer, the frequencies are 60.33%, 42.93%, 50.54%, 2.72%, 4.89% and 17.39% in MF, HT, RQ, KS, KEL and AKS respectively. Therefore, the frequencies of dust events south of the TB are obviously higher than those north of the TB. Here, dust events include dust storms and cases of blowing and floating dust, of these dust events, cases of floating dust occupy the majority, accounting for more than 50.00% in the south of the TB (Fig. 5b). The results above are consistent with the findings of Zhou et al. (2020), and the main reason is when the cold air streams of different intensities intrude, the wind fields converge strongly and rise in the HT and MF areas, thereby making these areas with the highest frequency of dust weather (Han et al., 2005).

The information on the dust top height (DTH) can help elucidate the vertical structure of dust. The DTH, which is defined as the height above surface elevation (a.s.e),

https://doi.org/10.5194/acp-2021-892
Preprint. Discussion started: 17 November 2021


Atmospheric Chemistry and Physics Discussions

shows significant seasonal variations over TB (Figs. 5c and 5d). The blank area is the default value of observation. Over the TB, the DTH was larger in spring compared to the summer, with the range of 2.0-5.5 km. Note that the variations here resembled those of the boundary layer height (BLH) (Luo et al., 2017). Previous study suggested that BLH was a key factor to determine the vertical distributions of dusts in the TB. Different from urban district (Ding et al. 2016; Huang et al. 2018; Li et al. 2021), the BLH was super high with over 5,000-m-depth in the TD based on the sounding data obtained from a month-long intensive field campaign carried out in July 2016 (Wang et al., 2019).

The results above indicate that spring and summer are the frequent seasons of dust weather in TB, especially in the south of the basin. Dust can suspend in the upper layer for a long time. Moreover, as an important component of absorbing aerosols, the dust aerosols could provide an elevated heat source to the air (Lau et al., 2006). Therefore, we reveal the contribution of the suspended dust to the anomalously warm layer over the TB based on the in-situ observation in the following.

3.3 Spatial and temporal features of the heating effect due to dust aerosols

Previous studies reported that the dust emitted from the TD has anomalously strong optical absorption properties and thus a more significant heating ability (Ge et al., 2010; Huang et al., 2015). In the following, based on the method proposed by Ding et al. (2013, 2016) using the temperature difference between the observation and reanalysis data (referred to as the OMR: observation minus reanalysis, see the section 2 Data and Methodology), the effects of dust aerosols on the temperature are estimated. Here, radiosonde observations and Fifth-Generation European Centre for Medium-Range Weather Forecasts (ECMWF) Reanalysis (ERA-5) reanalysis data are used.

In this study, we focus mainly on the temperature anomalies at altitudes of 500-300

https://doi.org/10.5194/acp-2021-892
Preprint. Discussion started: 17 November 2021


Atmospheric Chemistry and Physics Discussions

hPa. Fig.6 present vertical profiles of the temperature difference between the radiosonde observations and the ERA-5 data at altitudes of 500-300 hPa in spring and summer during 2016-2017. The ERA-5 reanalysis does not assimilate aerosol data (Ding et al., 2013, 2016), while radiosonde measurements include the influence of aerosols. Thus, the effect of aerosols on the temperature can be estimated by calculating the OMR. As shown in Fig. 6, dust can heat the layer at altitudes of 500-300 hPa in spring and summer over the TB, however, it shows obvious temporal and spatial variation characteristics.

In spring, all stations show the heating from 500 hPa to 300 hPa with the mean OMR of 0.30 K. In summer, the initial height of the heating layer is higher than that in spring at altitudes of 500-300 hPa, especially in HT and MF. The average OMRs present that the heating layer is between 400 hPa and 300 hPa with the mean intensity of 0.13 K. The results indicate that the heating intensity in summer is significantly weaker than that in spring.

In the south of TB, the average OMR of the heating layer in spring and summer are 0.31 K and 0.17 K, respectively. In the north of TB, the average OMR of the heating layer in spring and summer are 0.28 K and 0.12 K, respectively. Therefore, the heating intensity in the south is stronger than that in the north over the TB.

Although the heating effect of suspend dust is confirmed from the in-situ observation of the station, the dust heating of the whole basin cannot be obtained due to the limitation of the number of stations. Therefore, in order to solve this problem, we take the Modern-Era Retrospective Analysis for Research and Applications, Version 2 (MERRA-2) reanalysis data as the observation. The main reasons are as follows: firstly, one of the advances in MERRA-2 is the assimilation of aerosol observations, thereby it provides a multidecadal reanalysis in which aerosol and meteorological observations are jointly

https://doi.org/10.5194/acp-2021-892
Preprint. Discussion started: 17 November 2021


Atmospheric Chemistry and Physics Discussions

assimilated within a global data assimilation system (Gelaro et al., 2017). Secondly, Fig. 7a shows the relationship between atmospheric radiosonde temperature observations and MERRA-2 reanalysis data at altitudes of 500-300 hPa in spring and summer during 2016-2017. The linear fitting slopes between Atmospheric radiosonde temperature observations and MERRA-2 reanalysis data are 0.993 and 0.995 in 2016 and 2017, respectively, with the correlation coefficients (R^2) of 0.997. In addition, the mean square errors (MSE) of each layer between the radiosonde observation and MERRA-2 data at altitudes of 500-300 hPa in 2016-17 are obtained (Fig. 7b). The MSE is used to measure the deviation of two sets of data. It is found that the MSE of each layer is between 0.06 and 0.10. Therefore, it is feasible that we use MERRA2 data as observations to analyze the heating effect of suspend dust over the whole basin.

Figs. 7c and 7d show the distributions of OMR averaged over 500-300 hPa in spring and summer during 2016-2017. The mean OMRs at altitudes between 500 hPa and 300 hPa present relatively high values south of the TD in both spring and summer, which are basically consistent with the dust occurrence frequency (Figs. 5a and 5b). Accordingly, the heating intensity by dust is greater (with a maximum of approximately +0.45 K) in spring than in summer (with a maximum of approximately +0.25 K). In summary, dust aerosols can exert a heating effect and are attributable to the warming in the atmospheric layer between 500 hPa and 300 hPa over almost the entire TB. As illustrated above, the results clearly demonstrate that dust can heat the upper atmosphere over the TB. Suspended dust serves as a critical “bridge”. This is a unique atmospheric phenomenon in China.

Combined with Figs. 2 and 6, Table 2 shows the contribution of suspend dust to abnormal heating layer at altitudes of 500-300 hPa over TB, with the average contribution

https://doi.org/10.5194/acp-2021-892
Preprint. Discussion started: 17 November 2021


Atmospheric Chemistry and Physics Discussions

of 13.77% and 10.25% in spring and summer, respectively. It is obvious that the dust radiative forcing is one of the contributors for the warm layer over the TB. We find that the water vapor at the altitude of 4-7 km is nearly saturated at daytime over the TZ (Fig omitted), which is almost at the same height as the dust layer, the water vapor would absorb solar radiation and heat the atmosphere. Hence, the water vapor may be an important contributor for the warm layer over the TB. Furthermore, radiative properties of the surface, atmospheric trace gases and clouds also influence the aerosol-radiation interactions (IPCC, 2013). Therefore, the warm layer over the TB is the result of multiple factors. There are still many unknown issues, which are worthy to be further studied.

3.4 Concept of the northward extension of Tibetan heat source

Topographically, the TB is adjacent to the TP (Fig. 1), which acts as an elevated heat source in spring and summer (Duan et al., 2013; Wonsick et al., 2014). The warm atmospheric layer over the TB seems a northward extension of Tibetan heat source. Therefore, we put forward the concept of the Tibetan heat source's northward extension, which is illustrated in Fig. 8. Considering the important roles of the TP and TB in affecting the climate along the Silk Road Economic Belt (Liu et al., 2020; Zhao et al., 2020), more attention should be paid to the impact of the Tibetan heat source's northward extension on the regional climate. Moreover, the northward extension of the Tibetan heat source could be attributed to extreme weather. In recent years, heavy precipitation events have occurred frequently in Xinjiang, ie., the extreme precipitation event lasted for more than 100 h in KS, AKS and HT from May 15 to 21, 2018. During this extreme precipitation event, the precipitation broke the annual historical extremum in many places, seriously endangering the local economic development and people's lives. Northward extension of the Tibetan heat source and its thermal forcing effect on regional precipitation anomaly

https://doi.org/10.5194/acp-2021-892
Preprint. Discussion started: 17 November 2021


Atmospheric Chemistry and Physics Discussions

in spring and summer need further analysis, meanwhile, it is also a new issue to be studied. Therefore, an in-depth study of the influence of the Tibetan heat source's northward extension on the regional weather and climate needs to be performed in the future.

4 Conclusions

Dust aerosols can warm the climate (Figs. 6 and 7), but how much dust aerosols net influence global climate is highly uncertain (Penner, 2019). Aerosol-radiation interactions requires knowledge of the spectrally varying aerosol extinction coefficient, single scattering albedo, and phase function (McComiskey and Feingold, 2008; Loeb and Su, 2010; Kahn, 2012), which can in principle be estimated from the aerosol size distribution, shape, chemical composition and mixing state (Sicard et al., 2014; Lacagnina et al., 2015; Li and Sokolik, 2018). They lead to the large uncertainties in quantifying the dust radiative effect in the models. Different from other studies (Gu et al., 2006, 2016; Law et al., 2006; Huang et al., 2009), the in-situ observational evidences on dust aerosols' heating effect over TB for the first time in this study. Of course, although we have avoided these complex processes above, it is undeniable that errors still exist. The main conclusions are as follows:

A relatively warm layer is observed between 700 hPa and 300 hPa in the spring and summer over the TB. In this study, we focus on the temperature anomalies at altitudes of 500-300 hPa, the values of ΔT at each station are positive and range from 2.29 K to 2.73 K in spring. In comparison, ΔT is smaller in summer than in spring, varying from 1.21 K to 1.57 K.

Dust can heat the layer at altitudes of 500-300 hPa in spring and summer over the TB, which shows obvious temporal and spatial variation characteristics. The heating intensity in summer (with the mean OMR of 0.30 K) is significantly weaker than that in

https://doi.org/10.5194/acp-2021-892
Preprint. Discussion started: 17 November 2021


Atmospheric Chemistry and Physics Discussions

spring (with the mean OMR of 0.13 K). Over the south of TB, the average OMR of the heating layer in spring and summer are 0.31 K and 0.17 K, respectively. Comparatively, over the north of the TB, the average OMR of the heating layer in spring and summer are 0.28 K and 0.12 K, respectively. Dust radiative forcing is one of the contributors for the warm layer over the TB. Topographically, the TB is adjacent to the Tibetan Plateau (TP), which acts as an elevated heat source in spring and summer. The warm atmospheric layer over the TB seems a northward extension of Tibet heat source. Therefore, the concept of the northward extension of Tibetan heat source is proposed.

Code availability.

The data and data analysis method are available upon request.

Data Availability.

The ERA-5 reanalysis data were available at ECMWF (https://cds.climate.copernicus.eu/cdsapp#!/dataset/reanalysis-era5-pressure-levels-monthly-means?tab=form) and MERRA-2 reanalysis data were provided by NASA Goddard Earth Science Data and Information Services Center through the NASA GES DISC online archive (air temperature, https://goldsmr5.gesdisc.eosdis.nasa.gov/data/MERRA2_MONTHLY/M2IMNPASM.5.12.4/; dust mixing ratio, https://goldsmr5.gesdisc.eosdis.nasa.gov/data/MERRA2/M2I3NVAER.5.12.4/). The CALIPSO data were obtained from the National Aeronautics and Space Administration (NASA) Langley Research Center Atmospheric Sciences Data Center (https://www-calipso.larc.nasa.gov/products/lidar/browse_images/production/). The meteorological observation data were supplied by the National Meteorological Information Center (http://data.cma.cn/) under license and so cannot be made freely available.

https://doi.org/10.5194/acp-2021-892
Preprint. Discussion started: 17 November 2021

Atmospheric Chemistry and Physics Discussions

Supplement.

The supplement related to this article is available online at:

Author contributions.

Yu-zhi Liu designed the study and contributed ideas. Qing-zhe Zhu, Qing He and Fan Yang conducted the long-term measurements and provided the data. Cheng-long Zhou, Yu-zhi Liu and Tian-liang Zhao interpreted the data. Cheng-long Zhou contributed to the interpretation and writing of the manuscript with contributions from the coauthors.

Competing interests.

The authors declare no competing financial interests.

Acknowledgements.

The authors are grateful to the science teams for providing the accessible data products used in this study.

Financial support.

This work was supported by the National Natural Science Foundation of China (42030612) and jointly supported by the Strategic Priority Research Program of the Chinese Academy of Sciences (Grant No. XDA2006010301), National Natural Science Foundation of China (41905009, 91744311, 41991231, 91937302, 41875019, 41975010 and 41830968), and the Fundamental Research Funds for the Central Universities (lzujbky-2020-kb02).

Review statement.

This paper was edited by and reviewed by referees.

https://doi.org/10.5194/acp-2021-892
Preprint. Discussion started: 17 November 2021

Atmospheric Chemistry and Physics Discussions

References:

Cheng, Y.M., Dai, T., Li, J.M., and Shi, G.Y.: Measurement report: determination of aerosol vertical features on different timescales over East Asia based on CATS aerosol products, Atmos. Chem. Phys., 20, 15307-15322, https://doi.org/ 10.5194/acp-20-15307-2020, 2020.

Ding, A. J., Fu, C.B., Yang, X.Q., Sun, J.N., Petäjä, T., Kerminen, V.M., Wang, T., Xie, Y., Herrmann, E., Zheng, L.F., Nie, W., Liu, Q., Wei, X.L., and Kulmala, M.: Intense atmospheric pollution modifies weather: A case of mixed biomass burning with fossil fuel combustion pollution in eastern China, Atmos. Chem. Phys., 13, 10545-10554, https://doi.org/ 10.5194/acp-13-10545-2013, 2013.

Ding, A.J., Huang X., Nie, W., Sun, J.N., Kerminen, V.M., Petäjä, T., Su, H., Cheng, Y.F., Yang, X.Q., Wang, M.H., Chi, X.G., Wang, J.P., Virkkula, A., Guo, W.D., Yuan, J., Wang, S.Y., Zhang, R.J., Wu, Y.F., Song, Y., Zhu, T., Zilitinkevich, S., Kulmala, M., and Fu, C.B.: Enhanced haze pollution by black carbon in megacities in China, Geophy. Res. Lett., 43, 2873–2879, https://doi.org/ 10.1002/2016GL067745, 2016.

Duan, A. M., Wang, M. R., Lei, Y.H., and Cui, Y.F.: Trends in summer rainfall over china associated with the Tibetan Plateau sensible heat source during 1980–2008, J. Climate., 26, 261-275, https://doi.org/ 10.1175/JCLI-D-11-00669.1, 2013.

Ge, J.M., Su, J., Ackerman, T.P., Fu, Q., Huang, J.P., and Shi, J.S.: Dust aerosol optical properties retrieval and radiative forcing over northwestern China during the 2008 China-U.S. joint field experiment, J Geophys. Res., 115, D7, https://doi.org/ 10.1029/2009JD013263, 2010.

Ge, J.M., Huang, J.P., Xu, C.P., Qi, Y.L., and Liu, H.Y.: Characteristics of Taklimakan dust emission and distribution: a satellite and reanalysis field perspective, J Geophys.

https://doi.org/10.5194/acp-2021-892
Preprint. Discussion started: 17 November 2021

Atmospheric Chemistry and Physics Discussions

Res., 119, 11772-11783, https://doi.org/ 10.1002/2014JD022280, 2014.

Gelaro, R., and Coauthors.: The Modern-Era Retrospective Analysis for Research and Applications, Version 2 (MERRA-2), J. Climate., 30, 5419-5454, https://doi.org/ 10.1175/JCLI-D-16-0758.1, 2017.

Gong, S.L., Zhang, X.Y., Zhao, T.L., Mckendry, I.G., Jaffe, D.A., and Lu, N.M.: Characterization of soil dust aerosol in China and its transport and distribution during 2001 ACE-Asia: 2. model simulation and validation, J. Geophy. Res., 108, D9, https://doi.org/ 10.1029/2002JD002633, 2003.

Gu, Y., Liou, K.N., Xue, Y., Mechoso, C.R., Li, W., and Luo, Y.: Climatic effects of different aerosol types in China simulated by UCLA general circulation model, J Geophys. Res., 111, D15201, https://doi.org/10.1029/2005JD006312, 2006.

Gu, Y., Xue, Y., De Sales, F., and Liou, K.N.: A GCM investigation of dust aerosol impact on the regional climate of North Africa and South/East Asia, Clim. Dyn., 46, 2353-2370, https://doi.org/10.1007/s00382-015-2706-y, 2016.

Han, Y. X., Fang, X. M., Song, L. C., Zhang, Q., and Yang, S.L.: A Study of Atmospheric Circulation and Dust Storm Causes of Formation in the Tarim Basin-The Restructured Wind Field by Shapes of Dune and Observed Prevailing Wind, J Atmos Sci., 29, 627-635, https://doi.org/10.3878/j.issn.1006-9895.2005.04.14, 2005. (in Chinese)

Hersbach, H., and Coauthors.: The ERA5 global reanalysis, Q. J. R. Meteorol. Soc., 146, 1999-2049, https://doi.org/ 10.1002/qj.3803, 2020.

Huang, J., Bing, L., Minnis, P., Wang, T., Xin, W., Hu, Y., Yi, Y., and Ayers, J.K.: Satellite-based assessment of possible dust aerosols semi-direct effect on cloud water path over East Asia, Geophy. Res. Lett., 33, L19802., https://doi.org/ 10.1029/2006GL026561, 2006a.

https://doi.org/10.5194/acp-2021-892
Preprint. Discussion started: 17 November 2021


Atmospheric Chemistry and Physics Discussions

Huang, J., Minnis, P., Lin, B., Yi, Y., Sunmack, S., and Ayers, K.: Possible influences of Asian dust aerosols on cloud properties and radiative forcing observed from MODIS and CERES, Geophy. Res. Lett., 33, L06824, https://doi.org/ 10.1029/2005GL024724, 2006b.

Huang, J., Minnis, P., Chen, B., Huang, Z., Liu, Z., Zhao, Q., Yi, Y., and Ayers, J.: Long-range transport and vertical structure of Asian dust from CALIPSO and surface measurements during PACDEX, J. Geophys. Res., 113, D23212, https://doi.org/ 10.1029/2008JD010620, 2008.

Huang, J., Fu, Q., Su, J., Tang, Q., Minnis, P., Hu, Y., Yi, Y., and Zhao, Q.: Taklimakan dust aerosol radiative heating derived from CALIPSO observations using the Fu-Liou radiation model with CERES constraints, Atmos. Chem. Phys., 9, 4011-4021, https://doi.org/ 10.5194/acp-9-4011-2009, 2009.

Huang, J.P, Fu, Q., Zhang, W., Zhang, R., Ye, H., and Warren, S.: Dust and black carbon in seasonal snow across Northern China, B. Am. Meteorol. Soc., 92, 175-181, https://doi.org/10.1175/2010BAMS3064.1, 2011.

Huang, J., Wang, T., Wang, W., Li, Z., and Yan, H.: Climate effects of dust aerosols over east Asian arid and semiarid regions, J Geophys. Res., 119: 11398-11416, https://doi.org/ 10.1002/2014JD021796, 2015.

Huang X., Wang, Z.L., and Ding, A.J.: Impact of aerosol-PBL interaction on haze pollution: Multiyear observational evidences in North China, Geophys. Res. Lett., 45, 8596-8603, https://doi.org/10.1029/2018GL079239, 2018.

IPCC.: Climate Change 2013: The Physical Science Basis. Cambridge University Press, 604 pp, https://doi.org/10.1017/CBO9781107415324, 2013.

Luo, H., Han, Y., and Li, Y.: Temporal evolution of the boundary layer height and

https://doi.org/10.5194/acp-2021-892
Preprint. Discussion started: 17 November 2021

contribution of dust devils to dust aerosols, China Environ. Sci., 37, 2438–2442, 2017.

Jia, R., Liu, Y., Chen, B., Zhang, Z., and Huang, J.: Source and transportation of summer dust over the Tibetan Plateau, Atmos. Enviro., 123, 210-219, http://dx.doi.org/10.1016/j.atmosenv.2015.10.038, 2015.

Jia, R., Liu, Y., Hua, S., Zhu, Q., and Shao, T.: Estimation of the aerosol radiative effect over the Tibetan Plateau based on the latest CALIPSO product, J. Meteorol. Res., 32, 707-722, https://doi.org/ CNKI:SUN:QXXW.0.2018-05-003, 2018.

Kahn, R.: Reducing the uncertainties in direct aerosol radiative forcing, Surv. Geophys., 33, 701 – 721, https://doi.org/ 10.1007/s10712-011-9153-z, 2012.

Lacagnina, C., and Coauthors.: Aerosol single-scattering albedo over the global oceans: Comparing PARASOL retrievals with AERONET, OMI, and AeroCom models estimates, J. Geophys. Res., 120, 9814-9836, https://doi.org/10.1002/2015JD023501, 2015.

Lau, K.M., Kim, M. K., and Kim, K.M.: Asian summer monsoon anomalies induced by aerosol direct forcing: the role of the Tibetan Plateau, Clim. Dyn., 26, 855-864, https://doi.org/10.1007/s00382-006-0114-z, 2006.

Li, L., and Sokolik, I.N.: The dust direct radiative impact and its sensitivity to the land surface state and key minerals in the WRF‐Chem‐DuMo model: A case study of dust storms in Central Asia, J. Geophys. Res., 123, 4564-4582, https://doi.org/10.1029/2017JD027667, 2018.

Li, Q.H., Zhang, H.S., Cai, X.H., Song, Y., and Zhu, T.: The impacts of the atmospheric boundary layer on regional haze in North China, Npj-Clim. Atmos Sci., 4, 9, https://doi.org/10.1038/s41612-021-00165-y, 2021.

Liu, Y., Jia, R., Dai, T., Xie, Y., and Shi, G.: A review of aerosol optical properties and

https://doi.org/10.5194/acp-2021-892
Preprint. Discussion started: 17 November 2021


Atmospheric Chemistry and Physics Discussions

radiative effects, J. Meteorol. Res., 8, 1003-1028, https://doi.org/ 10.1007/s13351-014-4045-z, 2014.

Liu, Y., Sato, Y., Jia, R., Xie, Y., Huang, J., and Nakajima, T.: Modeling study on the transport of summer dust and anthropogenic aerosols over the Tibetan Plateau, Atmos. Chem. Phys., 15, 12581-12584, https://doi:10.5194/acp-15-12581-2015, 2015.

Liu, D., Zhao, T.L., Richard, B., Chen, S.Y., Lu, Z.Q., Wu, Y., and Zhao, Y.: Vertical Structures of Dust Aerosols over East Asia Based on CALIPSO Retrievals, Remote. Sens., 11, 701, https://doi.org/10.3390/rs11060701, 2019.

Liu, Y. Z., Li, Y. H., Huang, J.P., Zhu, Q.Z., and Wang, S.S.: Attribution of the Tibetan Plateau to northern drought, Natl. Sci. Rev., 7, 489-492, https://doi.org/ 10.1093/nsr/nwz191, 2020.

Loeb, N.G., and Su, W.Y.: Direct aerosol radiative forcing uncertainty based on a radiative perturbation analysis, J. Climate., 23, 5288–5293, https://doi.org/ 10.1175/2010JCLI3543.1, 2010.

McComiskey, A., and Feingold, G.: Quantifying error in the radiative forcing of the first aerosol indirect effect, Geophys. Res. Lett., 35, L02810, https://doi.org/ 10.1029/2007GL032667, 2008.

Penner, J.: Soot, sulfate, dust and the climate—Three ways through the fog, Nature., 570, 158–159, https://doi.org/10.1038/d41586-019-01791-6, 2019.

Randles, C.A., and Coauthors.: The MERRA-2 Aerosol Reanalysis, 1980 -- onward, Part I: System Description and Data Assimilation Evaluation, J. Climate., https://doi.org/ 10.1175/JCLI-D-16-0609.1, 2017.

Sicard, M., Bertolín, S., Mallet, M., Dubuisson, P., and Comerón, A.: Estimation of mineral dust long-wave radiative forcing: sensitivity study to particle properties and

https://doi.org/10.5194/acp-2021-892
Preprint. Discussion started: 17 November 2021


Atmospheric Chemistry and Physics Discussions

application to real cases in the region of Barcelona, Atmos. Chem. Phys., 14, 9213–9231, https://doi.org/10.5194/acp-14-9213-2014, 2014.

Simmons, A.: ERA-Interim: New ECMWF reanalysis products from 1989 onwards, ECMWF newslett., 110, 25–36, 2006.

Tsunematsu, N., Sato, T., Kimura, F., Kai, K., Kurosaki, Y., Nagai, T., Zhou, H., and Mikami, M.: Extensive dust outbreaks following the morning inversion breakup in the Taklimakan Desert, J. Geophys. Res., 110, D21207, https://doi.org/10.1029/2005JD005994, 2005.

Vaughan, M.A., Young, S.A., Winker, D.M., Powell, K.A., Omar, A.H., Liu, Z., Hu, Y., and Hostetler, C.A.: Fully automated analysis of space-based lidar data: an overview of the CALIPSO retrieval algorithms and data products, Laser Radar Tech. Atmos. Sens., 5575, 16–30, https://doi:10.1117/12.572024, 2004.

Wang, M.Z., Xu, X.D., Xu, H.X., Lenschow, D.H., Zhou, M.Y., Zhang, J.T., and Wang, Y.J.: Features of the deep atmospheric boundary layer over the Taklimakan Desert in the summertime and its influence on regional circulation, J Geophys. Res., 124, 12755-12772, https://doi.org/10.1029/2019JD030714, 2019.

Wang, S., Wang, J., Zhou, Z., and Shang, K.: Regional characteristics of three kinds of dust storm events in China, Atmos. Environ., 39, 509-520, https://doi.org/10.1016/j.atmosenv.2004.09.033, 2005.

Winker, D., Vaughan, M., and Hunt, B.: The CALIPSO mission and initial results from CALIOP, Proc. SPIE., 6409, 604902, https://doi:10.1117/12.698003, 2006.

Wonsick, M.M., Pinker, R.T., and Ma, Y.: Investigation of the "elevated heat pump" hypothesis of the Asian monsoon using satellite observations, Atmos. Chem. Phys., 14, 8749-8761, https://doi.org/ 10.5194/acp-14-8749-2014, 2014.

https://doi.org/10.5194/acp-2021-892
Preprint. Discussion started: 17 November 2021

Yang, M., Howell, S.G., Zhuang, J., and Huebert, B.J.: Attribution of aerosol light absorption to black carbon, brown carbon, and dust in China-interpretations of atmospheric measurements during EAST-AIRE, Atmos. Chem. Phys., 9, 2035-2050, https://doi.org/10.5194/acp-9-2035-2009, 2009.

Zhao, C. F., and Coauthors.: Aerosol characteristics and impacts on weather and climate over the Tibetan Plateau, Natl. Sci. Rev., 7, 492-495, https://doi.org/10.1093/nsr/nwz184, 2020.

Zhou, C., Yang, F., Mamtimin, A., Huo, W., Liu, X., He, Q., Zhang, J., and Yang, X.: Wind erosion events at different wind speed levels in the Tarim Basin, Geomorphology., 107386, https://doi.org/10.1016/j.geomorph.2020.107386, 2020.

https://doi.org/10.5194/acp-2021-892
Preprint. Discussion started: 17 November 2021


Atmospheric Chemistry and Physics Discussions

555 **Figure captions**

Figure 1. Topographical map of the study domain and distribution of observation stations in TB; the contours of the terrain height are in km (above mean sea level). The solid lines indicate the trajectory of the CALIPSO satellite over the TB on 4 July (20:22 UTC, black line), 5 July (07:02 UTC, red line), 25 July (20:40 UTC,
560 blue line,) and 27 July 2016 (20:28 UTC, green line), of which, 4 July and 5 July 2016 are dusty weather, 25 July and 27 July 2016 are clear day.

Figure 2. Temperature difference (ΔT) profiles in spring and summer during 2016-2017 at the (a) Kashi (KS), (b) Akesu (AKS), (c) Kuerle (KEL), (d) Hetian (HT), (e) Minfeng (MF), and (f) Ruoqiang (RQ) observation stations. The shading in (a-f)
565 indicates the layer with positive ΔT.

Figure 3. Averaged ΔT between 500 and 300 hPa in (a) spring and (b) summer. The position of the circle represents the site location, and the size of the circle represents the heating intensity.

Figure 4. The altitude-orbit cross-section of 532 nm total attenuated backscattering
570 intensity (left panels) and classified particles (right panels) on (a1 and b1) 4 July, (a2 and b2) 5 July, (a3 and b3) 25 July and (a4 and b4) 27 July 2016 along the trajectory of the CALIPSO satellite over the TP, as presented in Figure 1. The gray shading indicates the topography.

Figure 5. (a) Frequencies of dust events at the observation stations (KS, AKS, KEL, HT,
575 MF and RQ); (b) Frequencies of dust events including dust storms and cases of blowing and floating dust at the observation stations (KS, AKS, KEL, HT, MF and RQ) in spring and summer during 2016-2017. The blue dashed line represents the boundary between spring and summer; (c) Seasonal distribution

https://doi.org/10.5194/acp-2021-892
Preprint. Discussion started: 17 November 2021


Atmospheric Chemistry and Physics Discussions

of dust Top Height (km) obtained from CALIPSO data in spring over the TB; (d) Same as (c) but for summer.

Figure 6. Profiles of the temperature difference (radiosonde observation minus ERA-5 data) in spring and summer during 2016-2017 at (a) Kashi (KS), (b) Akesu (AKS), (c) Kuerle (KEL), (d) Hetian (HT), (e) Minfeng (MF) and (f) Ruoqiang (RQ).

Figure 7. (a) Relationship between atmospheric radiosonde temperature observations and MERRA-2 reanalysis data at altitudes of 500-300 hPa in spring and summer during 2016-2017; (b) the mean square errors (MSE) of each layer between the radiosonde observation and MERRA-2 data at altitudes of 500-300 hPa; and distributions of the temperature difference between MERRA-2 and ERA-5 data (OMR) averaged over 500-300 hPa in (c) spring and (d) summer during 2016-2017. The black solid circle represents the site location.

Figure 8. Conceptual scheme of the Tibetan heat source's northward extension partially attributed to the heating effect of suspended dust aerosols over the TB. Black lines denote the atmospheric temperature profile, in which the solid and dotted lines indicate the dust-influenced and dust-free profiles, respectively. Yellow arrows denote solar radiation, including the parts reflected and absorbed by clouds, dust aerosols and the surface. Red arrows at the surface denote the sensible heat. White solid arrows show the turbulence and convective mixing in the planetary boundary layer. White dashed lines show the altitude.

https://doi.org/10.5194/acp-2021-892
Preprint. Discussion started: 17 November 2021

Atmospheric Chemistry and Physics Discussions

Table 1. Fitting equations of each station based on the Eq. (1).

Station	Season	Fitting equation	
KS	Spring	$T_F = 0.117H - 77.564$	$R^2 = 0.983$
	Summer	$T_F = 0.109H - 64.468$	$R^2 = 0.994$
AKS	Spring	$T_F = 0.115H - 77.786$	$R^2 = 0.981$
	Summer	$T_F = 0.109H - 65.186$	$R^2 = 0.992$
KEL	Spring	$T_F = 0.113H - 77.682$	$R^2 = 0.981$
	Summer	$T_F = 0.110H - 65.349$	$R^2 = 0.992$
HT	Spring	$T_F = 0.117H - 76.374$	$R^2 = 0.981$
	Summer	$T_F = 0.106H - 60.881$	$R^2 = 0.988$
MF	Spring	$T_F = 0.117H - 76.382$	$R^2 = 0.981$
	Summer	$T_F = 0.106H - 60.502$	$R^2 = 0.986$
RQ	Spring	$T_F = 0.115H - 76.971$	$R^2 = 0.981$
	Summer	$T_F = 0.108H - 62.300$	$R^2 = 0.989$

605

610

https://doi.org/10.5194/acp-2021-892
Preprint. Discussion started: 17 November 2021

Atmospheric Chemistry and Physics Discussions

Table 2. Contribution of suspend dust to abnormal heating layer at altitudes of 500-300 hPa over TB.

Station	KS		AKS		KEL	
	Spring	Summer	Spring	Summer	Spring	Summer
Contribution	17.51%	29.00%	11.83%	7.87%	10.30%	3.16%
Station	HT		MF		RQ	
	Spring	Summer	Spring	Summer	Spring	Summer
Contribution	14.65%	4.06%	15.13%	6.94%	13.21%	10.46%

https://doi.org/10.5194/acp-2021-892
Preprint. Discussion started: 17 November 2021

Atmospheric Chemistry and Physics Discussions

630

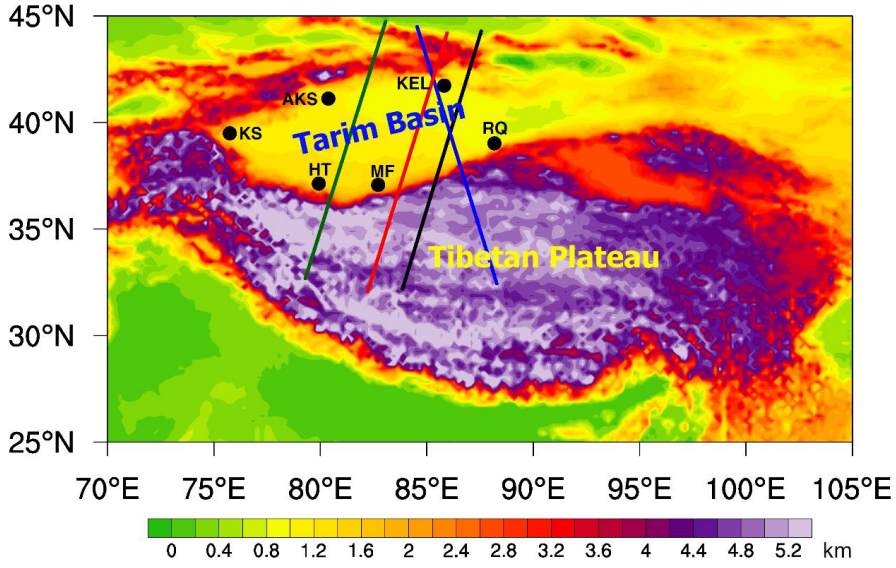

Figure 1. Topographical map of the study domain and distribution of observation stations in TB; the contours of the terrain height are in km (above mean sea level). The solid lines indicate the trajectory of the CALIPSO satellite over the TB on 4 July (20:22 UTC, black line), 5 July (07:02 UTC, red line), 25 July (20:40 UTC, blue line,) and 27 July 2016 (20:28 UTC, green line), of which, 4 July and 5 July 2016 are dusty weather, 25 July and 27 July 2016 are clear day.

635

640

https://doi.org/10.5194/acp-2021-892
Preprint. Discussion started: 17 November 2021

Atmospheric Chemistry and Physics Discussions

645

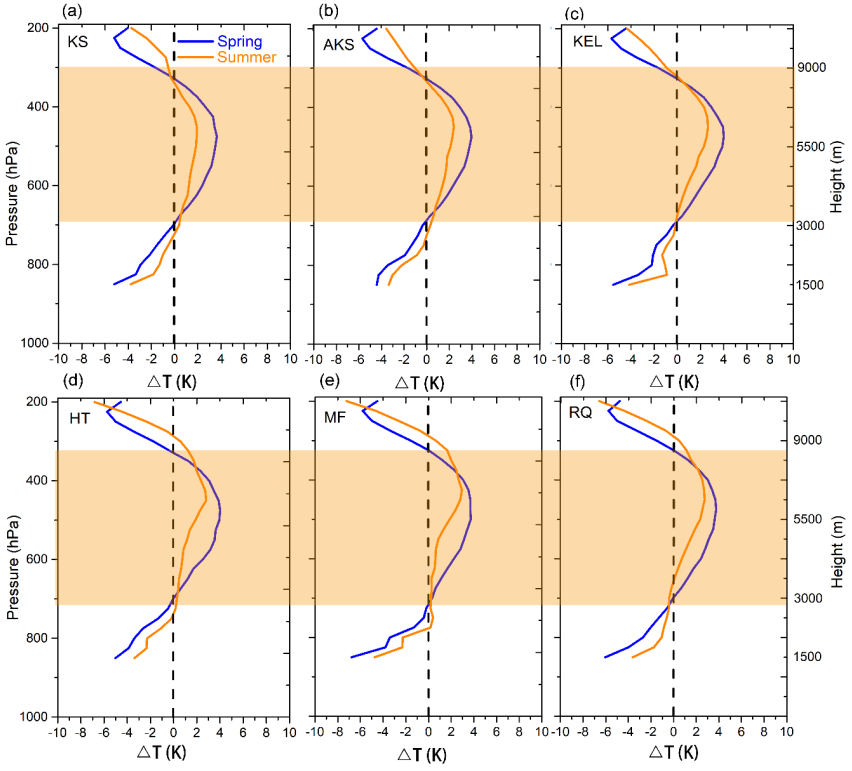

Figure 2. Temperature difference (ΔT) profiles in spring and summer during 2016-2017 at the (a) Kashi (KS), (b) Akesu (AKS), (c) Kuerle (KEL), (d) Hetian (HT), (e) Minfeng (MF), and (f) Ruoqiang (RQ) observation stations. The shading in (a-f) indicates the layer with positive ΔT.

650

655

https://doi.org/10.5194/acp-2021-892
Preprint. Discussion started: 17 November 2021

Atmospheric Chemistry and Physics Discussions

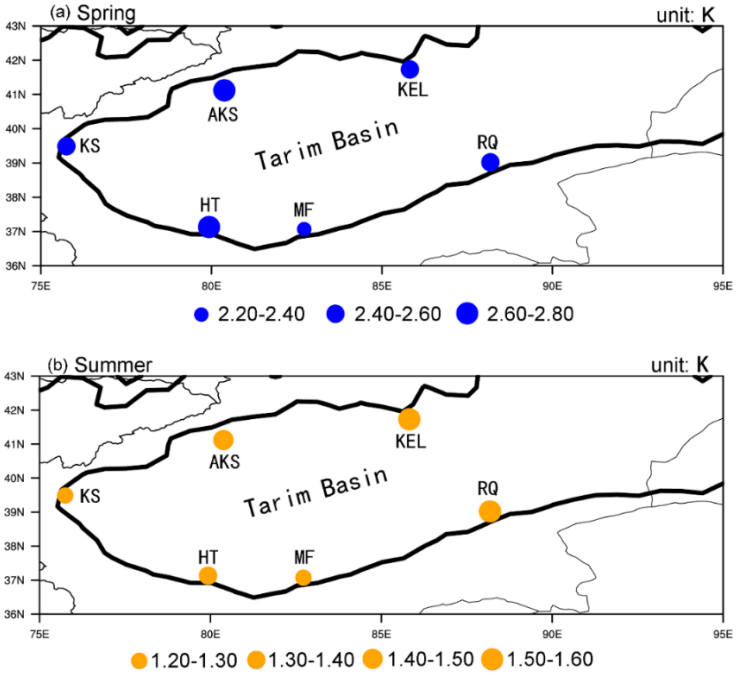

Figure 3. Averaged ΔT between 500 and 300 hPa in (a) spring and (b) summer. The position of the circle represents the site location, and the size of the circle represents the heating intensity.

https://doi.org/10.5194/acp-2021-892
Preprint. Discussion started: 17 November 2021

Atmospheric Chemistry and Physics Discussions

670

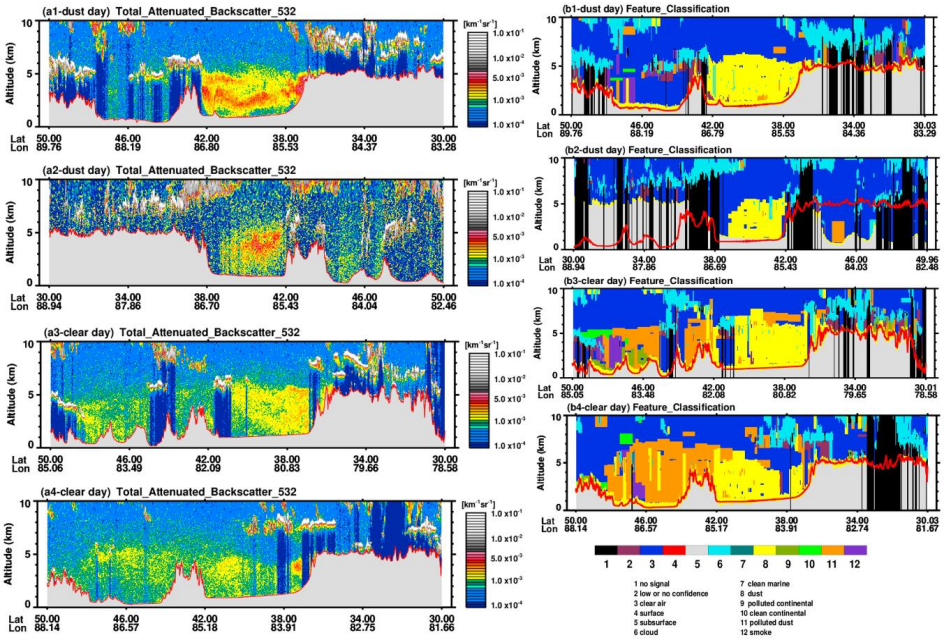

Figure 4. The altitude-orbit cross-section of 532 nm total attenuated backscattering intensity (left panels) and classified particles (right panels) on (a1 and b1) 4 July, (a2 and b2) 5 July, (a3 and b3) 25 July and (a4 and b4) 27 July 2016 along the trajectory of the CALIPSO satellite over the TP, as presented in Fig. 1. The gray shading indicates the topography.

675

680

https://doi.org/10.5194/acp-2021-892
Preprint. Discussion started: 17 November 2021

Atmospheric Chemistry and Physics Discussions

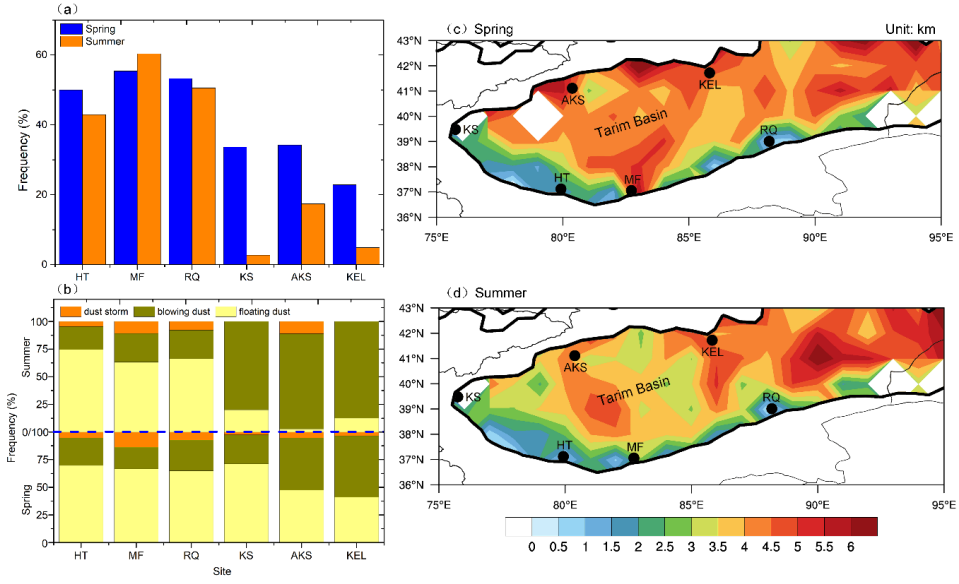

685

Figure 5. (a) Frequencies of dust events at the observation stations (KS, AKS, KEL, HT, MF and RQ); (b) Frequencies of dust events including dust storms and cases of blowing and floating dust at the observation stations (KS, AKS, KEL, HT, MF and RQ) in spring and summer during 2016-2017. The blue dashed line represents the boundary between 690 spring and summer; (c) Seasonal distribution of dust Top Height (km) obtained from CALIPSO data in spring over the TB; (d) Same as (c) but for summer.

695

https://doi.org/10.5194/acp-2021-892
Preprint. Discussion started: 17 November 2021

Atmospheric Chemistry and Physics Discussions

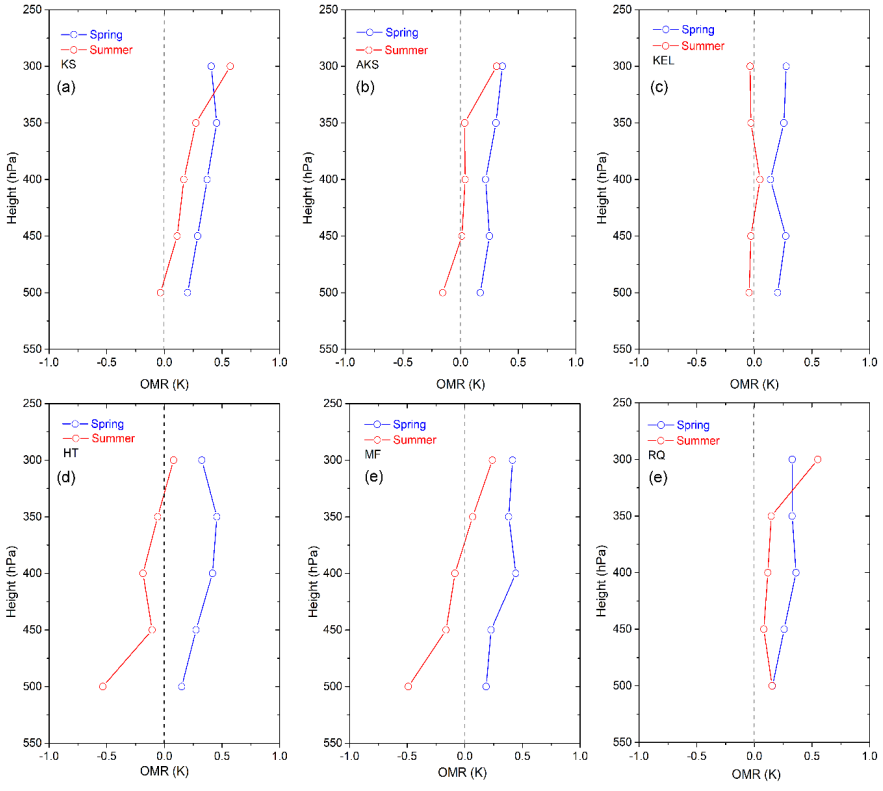

700

Figure 6. Profiles of the temperature difference (radiosonde observation minus ERA-5 data) in spring and summer during 2016-2017 at (a) Kashi (KS), (b) Akesu (AKS), (c) Kuerle (KEL), (d) Hetian (HT), (e) Minfeng (MF) and (f) Ruoqiang (RQ).

705

710

https://doi.org/10.5194/acp-2021-892
Preprint. Discussion started: 17 November 2021

Atmospheric Chemistry and Physics Discussions

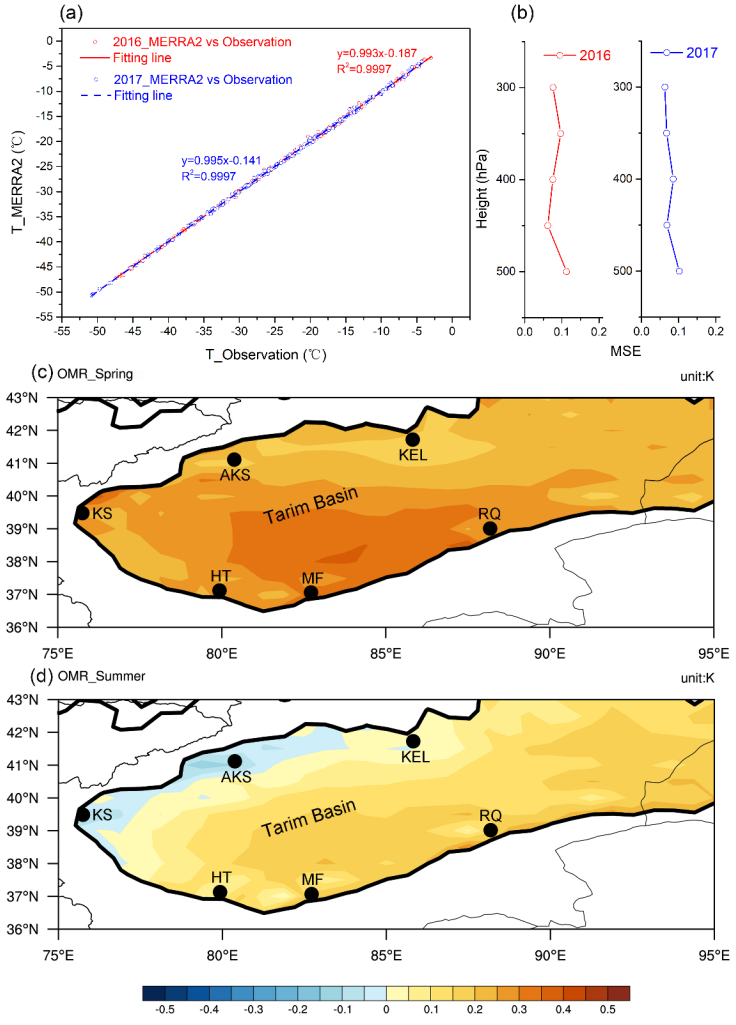

Figure 7. (a) Relationship between atmospheric radiosonde temperature observations and MERRA-2 reanalysis data at altitudes of 500-300 hPa in spring and summer during 2016-2017; (b) the mean square errors (MSE) of each layer between the radiosonde observation and MERRA-2 data at altitudes of 500-300 hPa; and distributions of the temperature difference between MERRA-2 and ERA-5 data (OMR) averaged over 500-300 hPa in (c) spring and (d) summer during 2016-2017. The black solid circle represents the site location.

https://doi.org/10.5194/acp-2021-892
Preprint. Discussion started: 17 November 2021

Atmospheric Chemistry and Physics Discussions

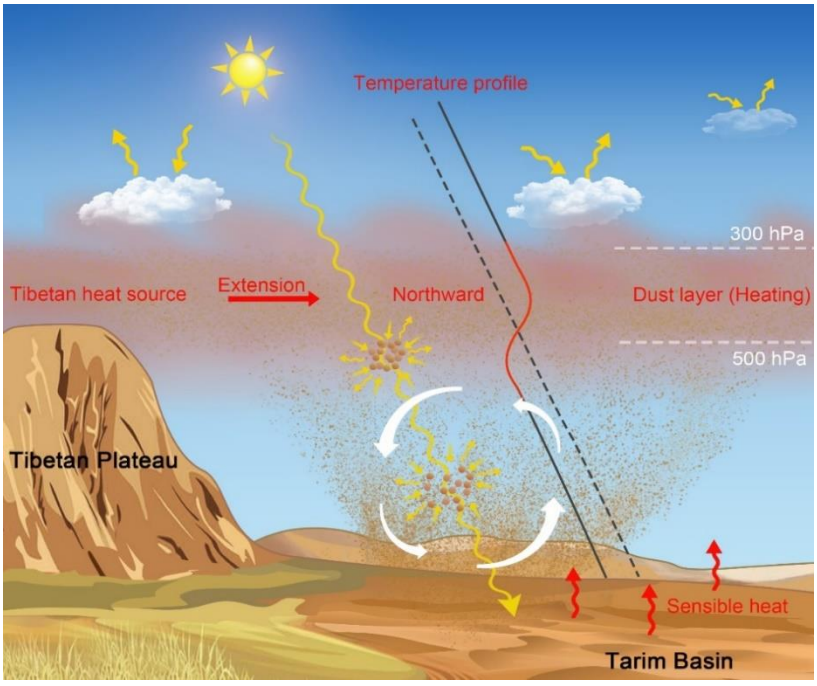

720

Figure 8. Conceptual scheme of the Tibetan heat source's northward extension partially attributed to the heating effect of suspended dust aerosols over the TB. Black lines denote the atmospheric temperature profile, in which the solid and dotted lines indicate the dust-influenced and dust-free profiles, respectively. Yellow arrows denote solar radiation, including the parts reflected and absorbed by clouds, dust aerosols and the surface. Red arrows at the surface denote the sensible heat. White solid arrows show the turbulence and convective mixing in the planetary boundary layer. White dashed lines show the altitude.

725